Journal of Computer-Aided Molecular Design, 10 (1996) 490–498
ESCOM

J-CAMD 349

Dimer asymmetry in superoxide dismutase studied by molecular dynamics simulation

Mattia Falconi[a,b,*], Ruggero Gallimbeni[b] and Emanuele Paci[c]

[a]*Department of Biology, University of Rome 'Tor Vergata', Via della Ricerca Scientifica e Tecnologica, I-00133 Rome, Italy*
[b]*Centre Européen de Calcul Atomique et Moleculaire (CECAM), École Normale Supérieure de Lyon, F-69364 Lyon, France*
[c]*SBPM/DBCM/DSV, CEA Centre d'Étude Saclay, F-91191 Gif-sur-Yvette Cédex, France*

Received 7 February 1996
Accepted 19 April 1996

Keywords: Cu,Zn superoxide dismutase; Molecular dynamics; Active site asymmetry; Atomic displacement covariance matrix

Summary

Molecular dynamics (MD) simulations of 100 ps have been carried out to study the active-site behaviour of the Cu,Zn superoxide dismutase dimer (SOD) in water. The active site of each subunit was monitored during the whole simulation by calculating the distances between functional residues and the catalytic copper. The results indicate that charge orientation is maintained at each active site but the solvent accessibility varies. Analysis of the MD simulation, carried out by using the atomic displacement covariance matrix, has shown a different intra-subunit correlation pattern for the two monomers and the presence of inter-subunit correlations. The MD simulation presented here indicates an asymmetry in the two active sites and different dynamic behaviour of the two SOD subunits.

Introduction

Cu,Zn superoxide dismutases are ubiquitous metalloenzymes that catalyse the dismutation of the superoxide anion (O_2^-), a toxic by-product of the oxygen metabolic cycle [1]. The steering of superoxide towards the active site of Cu,Zn superoxide dismutase dimers (SODs) has been shown, by experiment [2] and by simulation [3], to be modulated by an electrostatic recognition process.

The structure of bovine erythrocyte protein has been analysed by X-ray diffraction at 2 Å resolution [4] and atomic coordinates have been deposited in the Protein Data Bank [5] (entry code 2SOD). The four subunits, belonging to the two dimeric enzyme molecules deposited, have been named Orange/Yellow and Blue/Green. The folding of the dimer is globular and consists of two chemically equivalent subunits of 16 kDa (Fig. 1). Each subunit is composed of eight extended segments (β-strands) that form a flattened cylinder, called a β-barrel, and three external loops which form almost half of the subunit (Fig. 1). The β-barrel structure consists of two β-sheets: one is composed of four regular β-strands and the other of four twisted β-strands. In combination with the loops, the latter less regular β-sheet accommodates the active site. One loop (4,7) joins β-strands belonging to different sheets while the other two loops, larger and almost adjacent (loops 6,5 and 7,8), form a deep crevice connecting the solvent and the external surface of the barrel. Cu(II) and Zn(II) are located at the bottom of this channel: the Zn is buried and stabilises the protein structure, while the Cu is solvent accessible and catalytically active (Fig. 2a). The oxidised forms of five different species [4,6–9] and the reduced form of the bovine enzyme [10] have been thoroughly characterised by crystallographic analysis, showing that the two monomers have the same folding. However, also conserving the same topological fold, the root-mean-square (rms) deviation between the Orange and the Yellow monomers of the bovine enzyme is about 1.0 Å, indicating that the two structures are not completely identical.

One first-principle density functional theory calculation [11] and several molecular dynamics (MD) simulations have been carried out on the bovine Cu,Zn SOD, which have taken into account only one half of the dimer, the

*To whom correspondence should be addressed at: Department of Biology, University of Rome 'Tor Vergata', Via della Ricerca Scientifica e Tecnologica, I-00133 Rome, Italy.

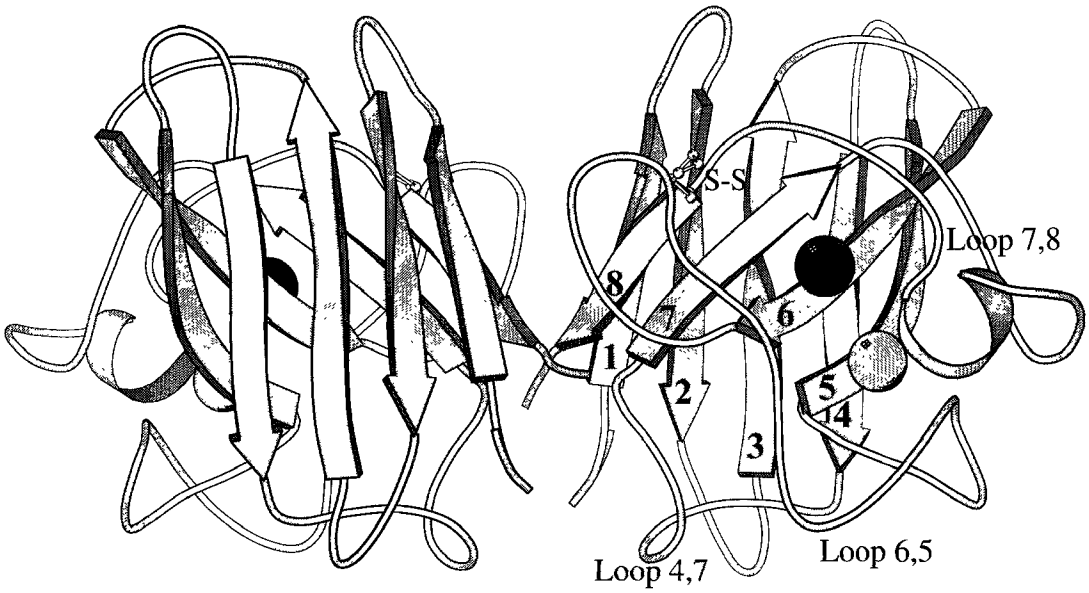

Fig. 1. Schematic view of the bovine Cu,Zn superoxide dismutase dimer. The arrows indicate the β-strands (β-strands 1,2,3,4 form the regular β-sheet while β-strands 5,6,7,8 form the irregular β-sheet). The three loops are represented as thin wires. The disulfide bridges (S-S) are indicated by the ball and stick representations. The black and grey spheres represent, respectively, the copper and the zinc ions. This picture was produced by MolScript, v. 1.4 (P.J. Kraulis, J. Appl. Crystallogr., 24 (1991) 946).

Orange subunit [12–17]. A possible functional interaction or structural asymmetry between the two subunits has never been considered in the previous MD calculations on Cu,Zn SOD.

In this paper we report an MD simulation carried out, for the first time, on the whole dimer of bovine Cu,Zn SOD in water. The aim of this work was to investigate the dynamic behaviour of the two SOD monomers to highlight the presence or the absence of communication between the two subunits.

Our simulation depicts a different average structure for each monomer and an intra-subunit atomic displacement covariance matrix (ADCM) pattern. Also we find a remarkable asymmetry in the shape of the channels connecting the surface of the protein to the active copper ion and the presence of correlations between the two subunits.

Methods

The MD simulation was performed using the computer program ORAC. The starting structure coordinates of the Orange/Yellow Cu,Zn SOD dimer at 2 Å resolution [4] were obtained from the Brookhaven Protein Data Bank [5]. A rectangular box with a volume of $43 \times 63 \times 35$ Å^3 was generated by translation of a primitive simple cubic

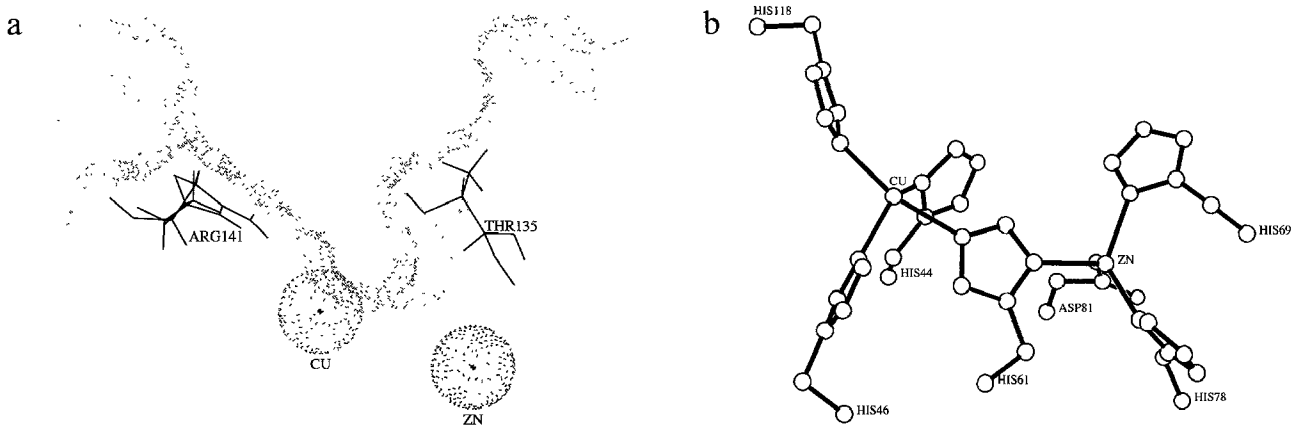

Fig. 2. (a) Cross section of the SOD active site. The diameter of the channel decreases stepwise towards the catalytic copper. Mobility of the residues Arg^{141} and Thr^{135}, forming the sides of the channel, can increase or decrease the availability of the copper ion for interaction with the superoxide. (b) Geometry of the active site metal ligands viewed from the solvent. The Cu ligands form a tetrahedrally distorted square plane while the Zn ligands form a tetrahedral with distortion towards a trigonal pyramid with Asp^{81} at the apex. The side chain of His^{61} forms a bridge between the Cu and the Zn ions. These molecular pictures were generated by Sybyl, v. 6.0 (Tripos Associates, St. Louis, MO, U.S.A.).

cell containing a water molecule to obtain a molecular lattice with a density of 1 g/cm^3 at 300 K. The protein, in its X-ray configuration with two crystal waters, was inserted in the centre of the water-filled simulation box. Only solvent molecules whose atoms were more than 90% the sum of the corresponding Lennard-Jones radii away from solute atoms were kept. With the remaining 1457 water molecules, the protein concentration was 17.5 mM. Four water molecules, chosen far enough from the active sites and the salt bridges, were replaced by sodium ions to make the system electroneutral. The system thus consisted of 7053 atoms, of which 2678 belonged to the protein itself (i.e. 2190 heavy atoms, 484 polar hydrogens, 2 copper and 2 zinc ions), 4371 were water molecules and 4 were sodium ions. All polar hydrogen atoms were included explicitly in the calculation, while those belonging to aliphatic and aromatic nonpolar groups were treated according to the united atom approximation [18]. The empirical simple point charge (SPC) model for water molecules [19] was used in the simulation. For dynamics integration, the Verlet algorithm [20] with a time step of 1 fs was used. All protein bond lengths were kept fixed by means of the SHAKE algorithm [21].

Potential function parametrisation

The functional form of the potential employed is the same as for the CHARMM force field [18]. We used the united atom potential parameter set labelled CHARMM20. For the metal clusters in the active sites (Fig. 2b) ab initio calculated atomic partial charges were used [22]. The metal ions were covalently bound to their ligand residue atoms but the flexibility of the active site bottom was preserved by assigning a zero value to the restoring force constant of angles and torsions that describe the coordination geometries. Lennard-Jones ε and σ parameters of zinc were used for copper and zinc ions. The two crystal waters close to the catalytic metals were considered as independent solvent molecules and were not bound to the copper ions. The other two histidines of the SOD subunit (His^{19} and His^{41}) were considered respectively neutral (Nδ1 atom protonated) and positive (Nδ1 and Nε2 atoms protonated) according to the hydrogen bond patterns given in the literature [4]. A group cutoff for electrostatic interactions of solute and solvent was employed; a nonbonded interaction spherical cutoff of 9.0 Å, smoothed by a cubic spline between 8 Å and the cutoff distance, was used.

Thermalisation and trajectory computations

The MD simulation was performed in the microcanonical ensemble. The energy of the system was roughly minimised in order to eliminate the overlap between atoms. At the beginning of the simulation the kinetic energy was set at 300 K by initialising the atomic velocities with a Boltzmann distribution. During the equilibration the temperature was periodically rescaled. The total potential energy reaches a plateau after about 140 ps. This behaviour signals that thermalisation has been achieved. After the

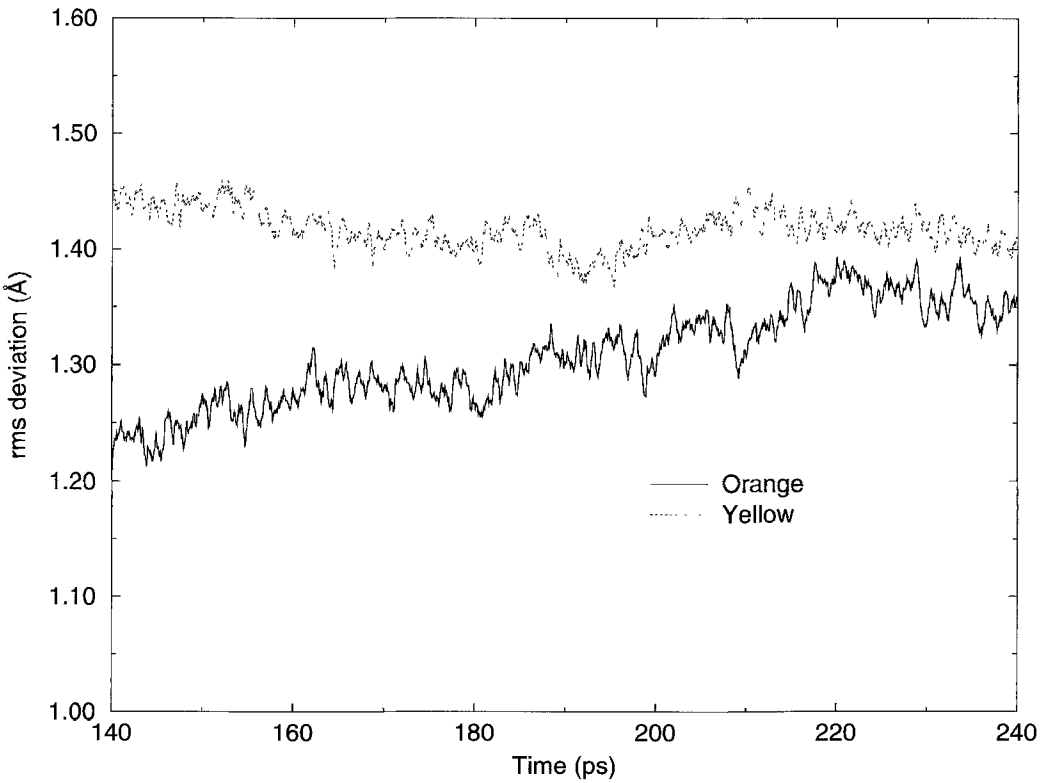

Fig. 3. X-ray root-mean-square deviation of the Orange and Yellow subunits during the trajectory.

equilibration we ran the system for a further 100 ps, collecting protein and solvent coordinates every 50 fs.

Atomic displacement covariance matrix

The dynamic behaviour of this protein in the MD simulation was analysed by using the ADCM to yield information about possible correlated motions [23 and the references therein]. Correlated motions can occur among proximal residues composing the subdomain regions of the Cu,Zn SOD subunit [24] but also between subdomains belonging to the same or to different subunits. The extent of correlated motions between residues is indicated by the magnitude of the corresponding correlation coefficient between their Cα atoms. The cross-correlation coefficient for the displacement of each pair of Cα atoms i and j is given by

$$c_{ij} = \frac{\langle \Delta \mathbf{r}_i \cdot \Delta \mathbf{r}_j \rangle}{\sqrt{\langle \Delta r_i^2 \rangle \langle \Delta r_j^2 \rangle}} \quad (1)$$

where Δr_i is the displacement from the mean position of the ith atom and the symbol $\langle\ \rangle$ represents the time average over the whole trajectory.

Results

The all-atom rms deviation from the crystal structure (X-rms) was computed by removing global translations and rotations and optimally superimposing, in a mean square sense, the instantaneous configurations with the reference one. The time dependence of the X-rms deviation for the two monomers during the trajectory is shown in Fig. 3. The X-rms deviation does not show a relevant drift along the trajectory and it is never larger than 1.4 and 1.5 Å for the Orange and the Yellow subunit respectively. Moreover, the calculated rms deviation between the two average subunit structures is 2.5 Å. This fact suggests that the two monomers have reached two different conformational substates during the simulation and are hence characterised by a different average structure.

Asymmetry in the active site opening motions

The active site opening motions in the two subunits were investigated by monitoring the distances from copper of the residues Arg^{141} [25] and Thr^{135} [26] which play a crucial role in the catalytic function. Both Thr^{135} and Arg^{141} constitute the walls of the narrowest portion of the catalytic funnel and limit access to the catalytic copper at the bottom of the active channel (see Fig. 2a). In Fig. 4a and b the distances from the copper of Nη1 and Nη2 atoms of the Arg^{141} guanidinium are reported for both subunits. In the crystallographic structure, the Nη2 atoms of Arg^{141} are close to the copper at a distance of approximately 5 Å in both subunits. During the thermalisation, in the Orange active site, atom Nη1 exchanges its position with Nη2 and gets close to the copper ion. This position is maintained during all the dynamics (Fig. 4a). On the other hand, in the Yellow subunit both Nη2 and Nη1 oscillate around a distance of about 11 Å from the copper (Fig. 4b). In the crystallographic structure, the distance Cu-Oγ1/Thr^{135} is about 5 and 7 Å in the Orange and Yellow subunit respectively. During the dynamics the Oγ1/Thr^{135} atom of the Orange subunit moves away from the copper atom and reaches a distance of about 10 Å, while the corresponding atom of the Yellow subunit moves nearer to the copper at a distance of about 5 Å.

The steric hindrance in the active site of the Orange subunit is therefore reduced with respect to the Yellow subunit, where the motions of residues Arg^{141} and Thr^{135} narrow the active site.

The behaviour of the solvent was monitored during the simulation to evaluate the interactions of bulk water with the copper active sites. Figure 5 shows the distance of the closest water molecule from the copper in both subunits. In the Orange site, after 18 ps, a water molecule reaches a distance of 2.9 Å from the copper and fluctuates around this distance for the remaining time of the simulation. On the contrary, during 100 ps no water molecules bind to the Yellow site. The distance of closest approach to the Cu is about 5 Å. However, the water molecules arriving at that distance exchange many times during the simulation with the bulk. To complete the picture, in the Yellow subunit only, the motion of the central part of loop 6,5, in the proximity of residue Pro^{60}, gives rise to a further reduction of the area accessible to the solvent* of the active site. The results listed in this paragraph indicate an active site asymmetry in the Cu,Zn SOD dimer. A stable orientation of the residues, which allows the access of water to the copper site, occurs only in the Orange active site. The fixed position of Arg^{141} guanidinium and the greater distance of the Thr^{135} oxydryl group generate a larger access area, which is in turn increased by the asymmetric fluctuations of loop 6,5. These arrangements allow the copper to get into contact with water and eventually with the substrate. Since it does not seem to occur in the Yellow subunit, the above observations suggest that the different substates, independently reached by the two monomers, are an indication of functional asymmetry.

Behaviour of the electrostatic residues

Residues Lys^{120}, Glu^{130}, Glu^{131} and Lys^{134} are known to play a dominant role in the electrostatic steering of the substrate [27 and the references therein].To focus on their behaviour in the simulation, we have monitored their distances from the copper. In both subunits Lys^{134} increases

*A solvent-accessible surface is the surface defined by a spherical probe with 1.4 Å radius rolled on the van der Waals surface of the protein [33].

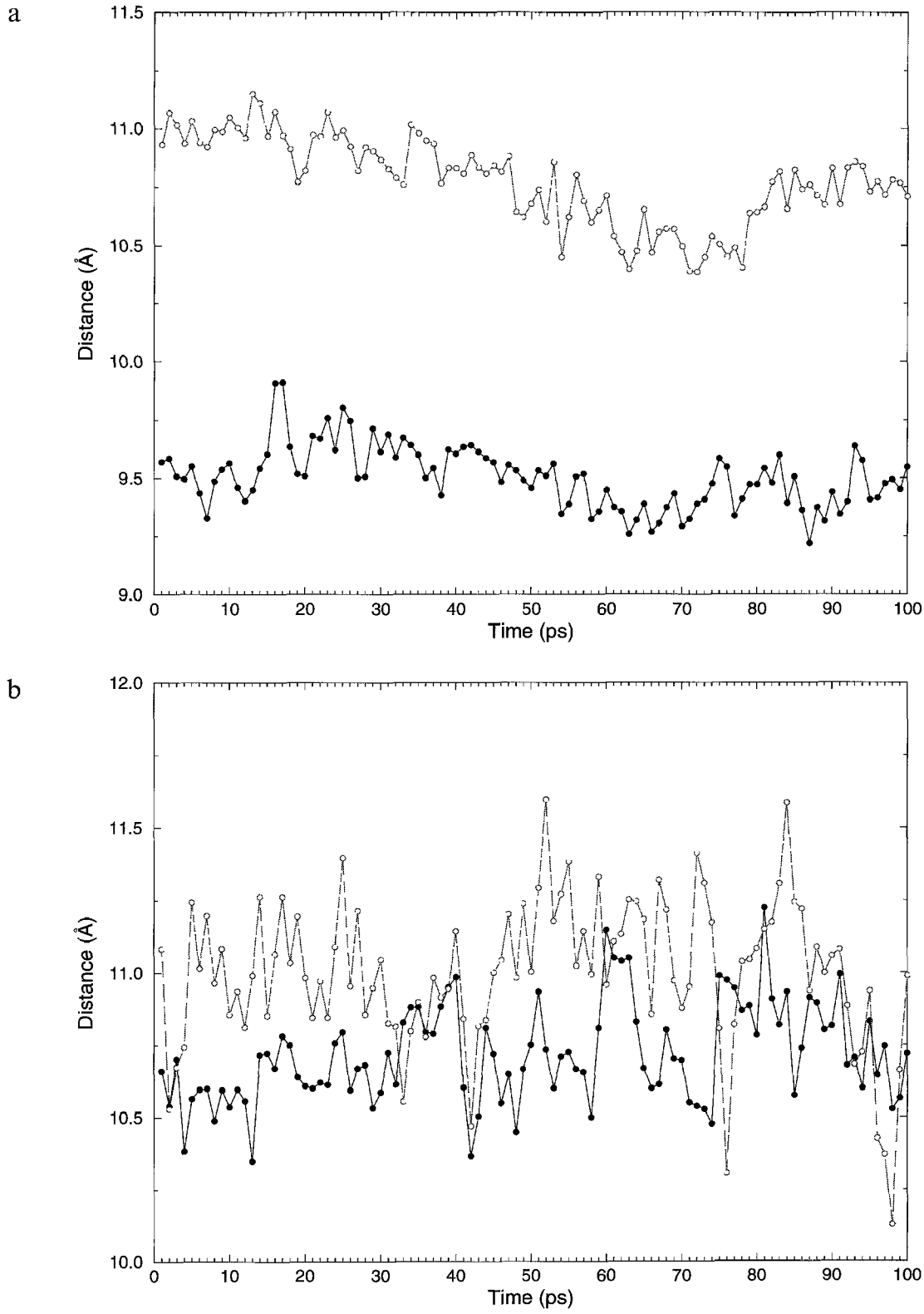

Fig. 4. Distances between copper and atoms Nη1 (black circles) and Nη2 (white circles) of Arg^{141} in the Orange subunit (a) and in the Yellow subunit (b) of SOD along the trajectory.

its copper distance with respect to that measured in the X-ray structure (from 7.6 to 12.2 Å and from 10.3 to 13.7 Å in the Orange and Yellow subunits) and establishes salt bridges with both Glu^{130} and Glu^{131}. In both subunits the Cδ atoms of Glu^{131} get closer to the copper compared to the distances observed in the crystal structure (from ca. 10 to 7 Å), while the Cδ atoms of Glu^{130} maintain the X-ray copper distance (about 16 Å). Glu^{131} is always oriented

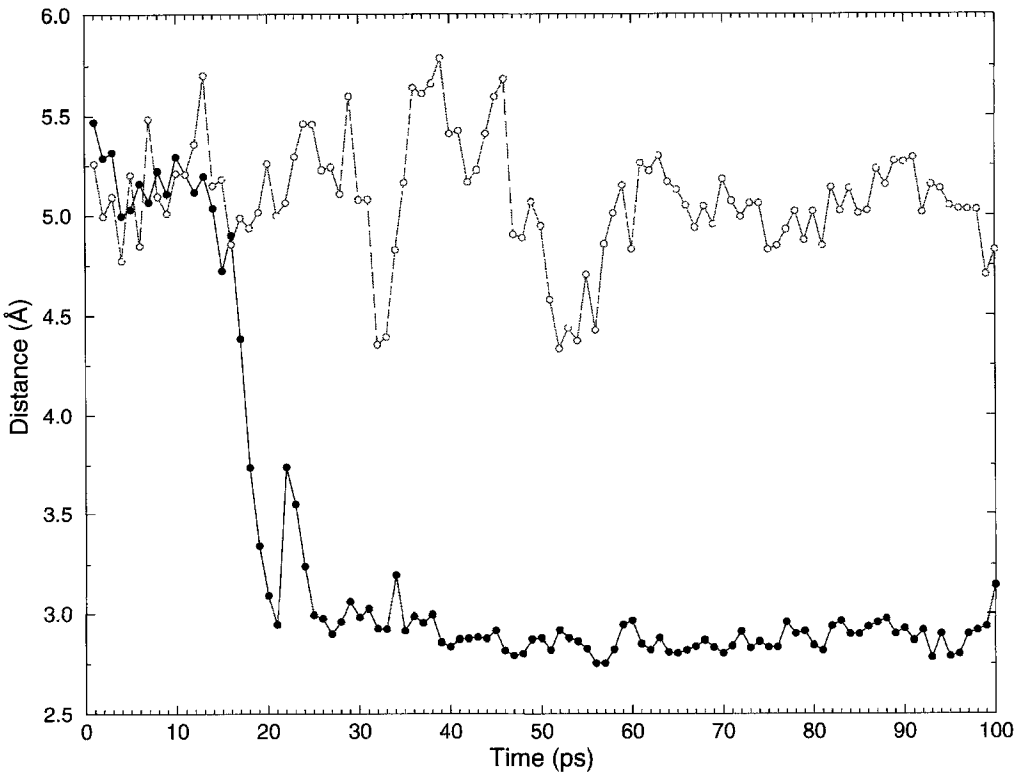

Fig. 5. Distance of the water oxygen closest to the copper in the Orange subunit (black circles) and in the Yellow subunit (white circles) of SOD along the trajectory.

towards the copper while Glu^{130} remains at the edge of the channel. This result complies with the major role proposed for Glu^{131} with respect to Glu^{130} in the electrostatic steering process [27]. In the Orange subunit the distance of Lys^{120} from copper is maintained with respect to that measured in the crystal structure (from 11.3 to 10.5 Å), while in the Yellow subunit this residue moves far away from its original X-ray position (from 12.8 to 16.9 Å). The amino acid residues Glu^{130}, Glu^{131} and Lys^{134} stabilise their opposite charges in the proximity of the copper through salt bridges, while Lys^{120} is free to fluctuate in a wide region around the channel. Brownian dynamics simulations indicate that Lys^{120} and Glu^{130} affect the electrostatic steering process in a general manner characteristic of a wide region surrounding the channel, while more dramatic effects were seen modifying the charges of Arg^{141}, Lys^{134} and Glu^{131} [28]. Moreover, Lys^{134} has been demonstrated to play a major role in the electrostatic guidance of superoxide in the active site [27]. The side-chain motions observed in this simulation show that the charge orientation, obtained by the salt bridge between residues Lys^{134} and Glu^{131}, is maintained in each active site, while the accessibility, due to the motions of Arg^{141} and Thr^{135}, is greater in the Orange subunit.

Concerning function, these results indicate that, due to the charged residues located by the border of the channel, the electrostatic driving force of the substrate remains constant in the two subunits and allows the approach of O_2^- towards the catalytic target. On the other hand, the conformation of the residues making up the internal walls of the channel changes, giving rise to the copper-superoxide interaction at the active site bottom.

Atomic displacement covariance matrix

Structural analysis of SOD indicates that each subunit is characterised by six subdomains [24]: the regular β-sheet, the irregular β-sheet, the Greek-key loop 4,7, the Zn-ligand region of loop 6,5, the disulfide region of loop 6,5 and the active site lid loop 7,8 (see Fig. 1). In order to verify the existence of correlations between the subdomains belonging to the same subunit or to different subunits of SOD, the atomic displacement covariance matrix has been calculated.

ADCM is represented as a two-dimensional plot in Fig. 6. To each pair of α-carbons (numbered from 1 to 151 for the Orange monomer and from 152 to 302 for the Yellow monomer) there corresponds a value of the ADCM. In the upper-left triangle of the plot, positive values have been represented by a black spot if they range between 0.6 and 1, and by a grey spot if they range between 0.2 and 0.6. Lower correlations correspond to empty spots. Absolute values of negative correlations are reported in the lower-right triangle using the same symbols described above for the positive correlations. A positive (or negative) correlation between the displacement of two α-carbon atoms with respect to their average position means

that the two sites move in phase (or in antiphase) along the same direction. As expected, the correlation between the adjacent α-carbons is very high and is represented by the black spots along the diagonal. High absolute values for the correlation are also found far from the diagonal of this map.

It is known [29] that high-order quantities, like the ADCM, are slow to converge. In order to check the convergence of the ADCM on a 100 ps run, we evaluated the same quantity on a completely independent trajectory of 120 ps [30] of the same system at very close external conditions (constant atmospheric pressure and constant 300 K temperature). For each i,j the estimation of the maximum error on C_{ij} is given by the difference of the two estimates of C_{ij} divided by 2. The maximum error computed in this way is narrowly distributed around zero. For 93% of the ij pairs, the error on C_{ij} is lower than 0.2 and it is never higher than 0.3 (while the maximum theoretical error is 1). The small difference between the two results shows that, in this simulation, pair correlation between atomic displacements has almost converged and the qualitative results described below do not strongly depend on the trajectory length.

The correlation spots scattered in squares I and IV represent, respectively, the positive and negative intersubunit correlations. In the upper-left panel (I) it can be noted that a turn region in the regular β-sheet (between the β-strands 2 and 3, residues 22–26) and the middle part of the Zn-ligand region of loop 6,5 (residues 72–75) of the Orange subunit (see Fig. 1) are positively correlated with various fragments scattered along the sequence of the Yellow subunit. The largest loop and the rigid β-scaffold of one SOD subunit are correlated with almost the entire structure of the other monomer. These protein regions, belonging to different subunits, move in phase.

The lower-left panel (II) shows the correlations in the Orange subunit. In particular, the disulfide region of loop 6,5 (residues 50–59) of the dimer interface is correlated with the β-strand 4 (93–102) belonging to the regular sheet of the β-barrel. Moreover, the middle part of loop 6,5 (60–71) is correlated with one extremity of the same loop (the Zn-ligand region 74–81), the central part of loop 4,7 (residues 108–109) and with almost all the residues belonging to the active site lid loop 7,8 (the electrostatic loop 123–138). The Zn-ligand region, the electrostatic loop and the middle part of loop 6,5 identify the active site of the SOD subunit.

These findings indicate that, in the Orange subunit, the interface region is correlated with a chain fragment far from the dimer contact and that correlated motions are involved in modelling the active site. The upper-right panel (III) shows the correlations in the structure of the Yellow subunit. The bend region including a connection between the regular and the irregular β-sheets (respective-

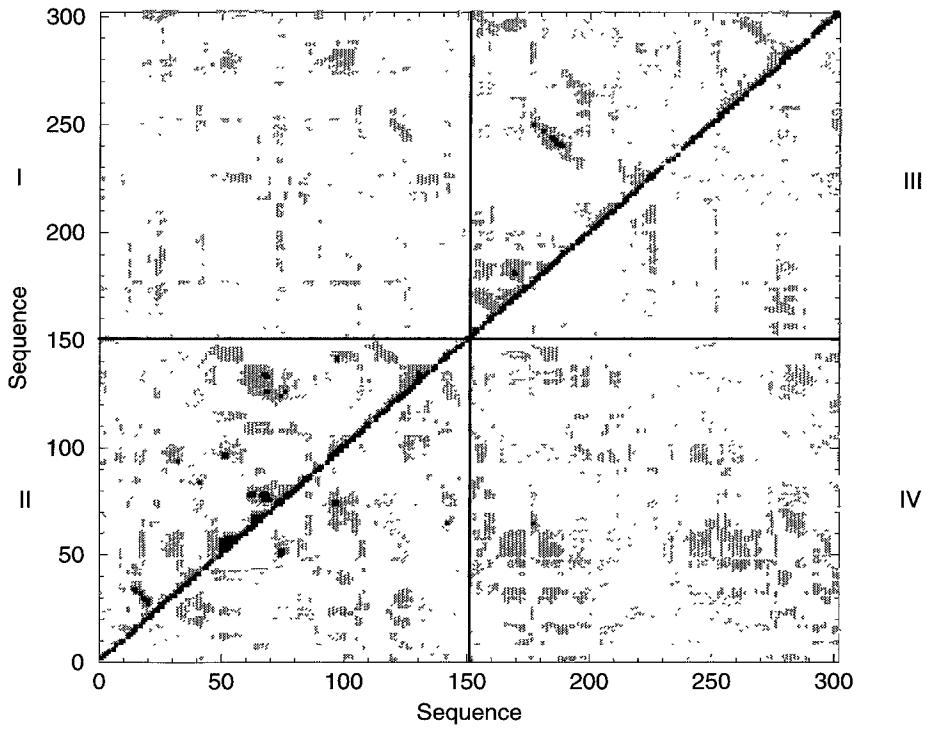

Fig. 6. Calculated atomic displacement covariance matrix for the Cu,Zn SOD dimer. The upper-left square (I) indicates the positive correlations between subunits. The lower-left square (II) indicates the positive and negative correlations (respectively upper-left and lower-right triangle) in the Orange subunit. The upper-right square (III) indicates the positive and negative correlations (respectively upper-left and lower-right triangle) in the Yellow subunits. The lower-right square (IV) indicates the negative correlations between subunits.

ly β-strands 3 and part of β-strand 6, residues 175–192) is correlated with a chain fragment including a turn and β-strand 4 (residues 237–252). This indicates that the motions of the regular β-sheet are correlated with those of the irregular one. There are large differences between the atomic displacement covariance matrix of the Orange and the Yellow subunits (panels II and III respectively).

The structure of the Yellow subunit appears to be less organised compared with the structure of the Orange subunit. The two monomers show different dynamic characteristics: in the Yellow subunit there are correlations between the two β-sheets, while in the Orange subunit correlations are found between the opposite sides of the monomer and between regions composing the active site. In both the subunits high correlations are found between the contiguous β-strands 1 and 2.

The lower-left panel (IV) shows the negative correlations between the subunits. In this case the disulfide region of loop 6,5 (residues 49–61) and the regular β-strand 4 (residues 92–101) of the Orange subunit are correlated with various chain fragments scattered along the sequence of the Yellow subunit.

As observed in panel I, the rigid motions of the β-structure framework and the motions involving the interface loop region of the Orange subunit are correlated with the motions of various chain fragments of the other subunit. Complex motions of noncovalently bound atoms generate strong, phase or antiphase, coupling between chain fragments distributed in the dimeric structure.

Panels I and IV highlight the presence, in this MD simulation, of weak correlations between specific regions of the well-structured Orange subunit and various regions scattered along the sequence of the Yellow subunit. These correlations can contribute to generate the different patterns of intra-subunit correlations observed in panels II and III.

Discussion

The active site asymmetry that is observed is the result of concerted motions of several amino acid residues that organise the active site of the Orange subunit to allow the interaction of superoxide with copper. This residue arrangement does not occur in the Yellow subunit. This result confirms the data previously obtained by other authors who have carried out MD simulations on the Orange subunit [12–17]. In three of these MD studies [12–14] the motions of the active site and the corresponding path followed by the superoxide approaching the copper ion have been analysed. Trajectory analysis revealed that the superoxide is directed toward the catalytic metal through the concomitant motions of several active site invariant residues. The significant role of protein fluctuations in the enzyme–substrate interactions has been confirmed by a study combining the use of Brownian and molecular dynamics in the presence of the substrate [15] and by MD calculations carried out on homology models of human Cu,Zn SOD mutants [16,17]. A common aspect stems from these dynamic simulations: the existence of a series of concerted motions that organise, sterically and energetically, the active site for the catalytic event.

The presence of the second subunit, which was not taken into account in the other simulations, gives new insight into the molecular dynamics picture of Cu,Zn SOD. In fact, the differences observed in the intra-subunit atomic displacement covariance matrices are an indication of different dynamic behaviours of the two subunits that sample different conformational substates, while the presence of correlations, observed calculating the inter-subunit ADCMs, indicates that a complex motion mechanism correlates the two monomers.

Some experimental data confirm this hypothesis and provide evidence for communication between the subunits. A conformational communication between the two subunits has been reported to occur in the process of metal reconstitution of the copper-depleted enzyme [31]. The distribution of the metal fits a model of cooperative interaction between the two sites. Occupation of the first site lowers the activation energy of the binding of the second Cu(II) ion. Evidence for the communication between the monomers also comes from the study of subunit-destabilising mutations in *Drosophila* Cu,Zn superoxide dismutase [32]. In this paper a dimer 'disequilibrium' model has been proposed in which mutant subunits alter the function of wild-type subunits in heterozygotes.

Conclusions

Analysis of the MD calculation indicates the existence of correlations between the two subunits which results in an asymmetry between the two SOD monomers. From the experimental data it is known that the conformational communications between the monomers could change the active site characteristics [31] and that the interaction between the subunits is crucial for the catalytic event [32]. Moreover, as observed by previous calculations, a precise organisation of the active site is necessary to fulfil the catalytic task [12–17].

On the basis of such considerations, it can be hypothesised that a communication between the subunits of Cu,Zn superoxide dismutase can contribute to modify the functional residue positions and reduce the free energy barriers that partially prevent the entrance of the superoxide in the active site.

Acknowledgements

The simulations on which the present results are based were executed at CECAM (Centre Européen de Calcul Atomique et Moleculaire), École Normale Supérieure,

Lyon (France). We gratefully acknowledge encouragement and guidance from Dr. M. Marchi. The authors are also grateful to Prof. G. Ciccotti, Prof. A. Desideri and Prof. G. Rotilio for useful discussions. This work was supported by the E.C. program 'Human Capital and Mobility' and by the National Research Council special project 'Struttura e Meccanismi di Funzionamento di Macromolecole Biologiche'. Two of us (M.F. and R.G.) were 'Human Capital and Mobility' fellowship holders.

References

1 Halliwell, B. and Gutteridge, J.M.C., Methods Enzymol., 186 (1990) 1.
2 Argese, E., Viglino, P., Rotilio, G., Scarpa, M. and Rigo, A., Biochemistry, 26 (1987) 3224.
3 Desideri, A., Falconi, M., Polticelli, F., Bolognesi, M., Djinovic, K. and Rotilio, G., J. Mol. Biol., 223 (1992) 337.
4 Tainer, J.A., Getzoff, E.D., Beem, K.M., Richardson, J.S. and Richardson, D.C., J. Mol. Biol., 160 (1982) 181.
5 Bernstein, F., Koetzle, T., Williams, G., Meyer Jr., E., Brice, M., Rodgers, J., Kennard, O., Shimanouchi, T. and Tasumi, M., J. Mol. Biol., 112 (1977) 535.
6 Kitagawa, Y., Tanaka, N., Hata, Y., Kusunoki, M., Lee, G., Katsube, Y., Asada, K., Aibara, S. and Morita, Y., J. Biochem., 109 (1991) 477.
7 Djinovic, K., Gatti, G., Coda, A., Antolini, L., Pelosi, G., Desideri, A., Falconi, M., Marmocchi, F., Rotilio, G. and Bolognesi, M., J. Mol. Biol., 225 (1992) 791.
8 Parge, H.E., Hallewell, R.A. and Tainer, J.A., Proc. Natl. Acad. Sci. USA, 89 (1992) 6109.
9 Djinovic-Carugo, K., Battistoni, A., Carri, M.T., Polticelli, F., Desideri, A., Rotilio, G., Coda, A., Wilson, K.S. and Bolognesi, M., Acta Crystallogr., D52 (1996) 176.
10 Rypniewsky, W.R., Mangani, S., Bruni, B., Orioli, P.L., Casati, M. and Wilson, K.S., J. Mol. Biol., 251 (1995) 282.
11 Carloni, P., Blochl, P.E. and Parrinello, M., J. Phys. Chem., 99 (1995) 1338.
12 Shen, J., Subramaniam, S., Wong, C.F. and McCammon, A., Biopolymers, 28 (1989) 2085.
13 Shen, J. and McCammon, A., Chem. Phys., 158 (1991) 191.
14 Wong, Y., Clark, T.W., Shen, J. and McCammon, A., Mol. Simul., 10 (1993) 277.
15 Luty, B.A., El Amrani, S. and McCammon, A.J., J. Am. Chem. Soc., 115 (1993) 11874.
16 Banci, L., Carloni, P., La Penna, G. and Orioli, P.L., J. Am. Chem. Soc., 114 (1992) 6994.
17 Banci, L., Carloni, P. and Orioli, P.L., Proteins, 18 (1994) 216.
18 Brooks, B.R., Bruccoleri, R.E., Olafson, B.D., States, D.J., Swaminathan, S. and Karplus, M., J. Comput. Chem., 4 (1983) 187.
19 Berendsen, H.J.C., Postma, J.P.M., Van Gunsteren, W.F. and Hermans, J., In Pullman, B. (Ed.) Intermolecular Forces, Reidel, Dordrecht, The Netherlands, 1981, pp. 331–342.
20 Verlet, L., Phys. Rev., 159 (1967) 98.
21 Ryckaert, J.P., Ciccotti, G. and Berendsen, H.J.C., J. Comput. Phys., 23 (1977) 327.
22 Shen, J., Wong, C.F., Subramaniam, S., Albright, T.A. and McCammon, J.A., J. Comput. Chem., 11 (1990) 346.
23 Komeiji, Y., Uebayasi, M. and Yamato, I., Proteins, 20 (1994) 248.
24 Getzoff, E.D., Hallewell, R.A. and Tainer, J.A., In Inouye, M. and Sarma, R. (Eds.) Protein Engineering, Academic Press, New York, NY, U.S.A., 1986, pp. 41–69.
25 Fisher, C.L., Cabelli, D.E., Tainer, J.A., Hallewell, R.A. and Getzoff, E.D., Proteins, 19 (1994) 24.
26 Getzoff, E.D., Cabelli, D.E., Fisher, C.L., Parge, H.E., Viezzoli, M.S., Banci, L. and Hallewell, R.A., Nature, 358 (1992) 347.
27 Polticelli, F., Bottaro, G., Battistoni, A., Carri, M.T., Djinovic-Carugo, K., Bolognesi, M., O'Neill, P., Rotilio, G. and Desideri, A., Biochemistry, 34 (1995) 6043.
28 Sines, J.J., Allison, S.A. and McCammon, J.A., Biochemistry, 29 (1990) 9403.
29 Clarage, B.J., Romo, T., Andrews, B.K., Pettitt, M. and Phillips Jr., G.N., Proc. Natl. Acad. Sci. USA, 92 (1995) 3288.
30 Paci, E. and Marchi, M., J. Phys. Chem., 100 (1996) 4314.
31 Rigo, A., Viglino, P., Bonori, M., Cocco, D., Calabrese, L. and Rotilio, G., Biochem. J., 169 (1978) 277.
32 Philips, J.P., Tainer, J.A., Getzoff, E.D., Boulianne, G.L., Kirby, K. and Hilliker, A.J., Proc. Natl. Acad. Sci. USA, 92 (1995) 8574.
33 Richards, F.M., Annu. Rev. Biophys. Bioeng., 6 (1977) 151.